Rapid Communications

Transitional region of a round synthetic jet

Xi Xia[1] and Kamran Mohseni[1,2,*]

[1]*Department of Mechanical and Aerospace Engineering, University of Florida, Gainesville, Florida 32611, USA*

[2]*Department of Electrical and Computer Engineering, University of Florida, Gainesville, Florida 32611, USA*

(Received 3 October 2017; published 22 January 2018)

Spreading and decay rates of several synthetic jets are experimentally measured up to 70–100 diameters (d) away from the orifice. It is found that, consistent with previous studies, after $10d$–$15d$ from the nozzle a synthetic jet displays a self-similar velocity profile together with enhanced spreading and decay behaviors than a continuous jet. However, this enhancement does not persist throughout the downstream region, as the spreading and decay rates around $30d$–$50d$ away from the orifice decrease to asymptotic values that are comparable to continuous jets. This intermediate region with enhanced spreading and decay rates is dubbed the transitional region, while the region beyond $30d$–$50d$, where the spreading and decay rates approach the continuous jet values, is referred to as the actual far field of a synthetic jet. Physically, the enhanced spreading and decay rates of the transitional region are caused by an enhanced mode of mixing related to the forced instability of the pulsed large vortices, which eventually break down into smaller eddies in the fully turbulent far field.

DOI: 10.1103/PhysRevFluids.3.011901

A synthetic jet [1–4] is also known as a zero-net-mass-flux (ZNMF) jet [5] or vortex generator jet [6]. Synthetic jets are typically created by a periodic process of fluid ingestion and expulsion, which leads to the generation of vortex rings or pairs [7–10]. Due to the advantages of ZNMF and enhanced mixing [5,11,12] compared with continuous jets, synthetic jets have been largely employed in applications of flow control [13–19], underwater vehicle propulsion [20,21], and cooling [22–25].

The flow field of a synthetic jet is commonly divided into a near field and a far field [5,7,26]. The near field is dominated by strong vortex rings and is pulsatile in nature, while the far field is characterized by self-similar velocity profiles that resemble a continuous turbulent jet [5,7,12,26–28]. For round synthetic jets, Rathnasingham and Breuer [27] and Mallinson *et al.* [28] found that the self-similar flow is achieved approximately at an axial distance of ten orifice diameters (d); a slightly larger distance ($15d$) was reported by Cater and Soria [5]. Based on the self-similar velocity profile, one may estimate the rate of change of the jet width in the streamwise direction, formally known as the spreading rate. A prominent observation from previous experimental studies [5,26,29–31] is that the spreading rate of a round synthetic jet is generally higher than that of a continuous turbulent jet; similar enhanced spreading rates have also been confirmed for two-dimensional synthetic jets [7,12]. In this Rapid Communication, we experimentally investigate the spreading and decay behaviors of different round synthetic jets, and find that at axial locations of $30d$–$50d$ the enhanced spreading and decay rates decrease to asymptotic values comparable to those of continuous jets. This indicates the existence of an extended transitional region beyond the near field, which should be distinguished from the fully developed far field of synthetic jets, although the self-similarity establishes from only about $10d$–$15d$ away.

*mohseni@ufl.edu

TABLE I. Test matrix for six sample synthetic jets. The complete parameter set for the 50 tested synthetic jets was reported in Ref. [32]. d is the orifice diameter, f is the driving frequency, L/d is the stroke ratio, and Re_s [26] is the Reynolds number estimated at the jet exit.

Case	d (mm)	f (Hz)	L/d	Re_s
SJ3	1.0	1750	24.6	4064
SJ9	1.0	1850	48.6	8476
SJ17	1.5	1850	14.8	5814
SJ23	1.5	1950	9.2	3825
SJ33	2.0	1850	4.7	3284
SJ45	2.0	1950	3.2	2389

In this Rapid Communication, we utilize the same experimental approach outlined in Ref. [32] for measuring the flow field of a synthetic jet. For our experiment, the test section was enclosed by a 61.0 cm × 61.0 cm × 91.4 cm container of plexiglass to isolate any drift flow from the outside. By adjusting the size of this enclosure, the current dimensions of the test section were testified to be sufficiently large such that the enclosure itself does not induce an additional disturbance to the jet flow. A constant-temperature hot-wire anemometry system was employed to sample the mean jet flow. Synthetic jets were created by a flat, hollow, cylindrical actuator with a piezoelectric disk on one side and a round orifice on the other. Three different synthetic jet actuators were tested with orifice diameter sizes of 1.0, 1.5, and 2.0 mm, respectively. By adjusting the sinusoidal voltage signal applied across the piezoelectric disk, the frequency f and stroke length L of a synthetic jet could be controlled. A total of 50 different synthetic jets were tested and the parameters for six sample cases are listed in Table I. To resolve the vortical structures in the jet flow, a particle image velocimetry (PIV) system was also employed. As has been introduced in Ref. [33], this PIV system consists of a high-speed complementary metal-oxide semiconductor (CMOS) camera (Phantom v210), a 20 mJ Nd:YLF laser (Quantronix Darwin Duo), and a TSI synchronizer. The trigger for the synthetic jet was synchronized with the PIV system and the trigger delay was adjusted to provide the desired phase-locked flow field (16 phases per cycle). The image pairs were acquired at a rate of $f/25$ for 2 s, with a total of 148 image pairs ($f = 1850$ Hz) sampled for each phase. The Insight 4G software by TSI, Inc. was used for data acquisition and postprocessing.

As introduced above, a self-similar velocity profile for a synthetic jet is usually achieved about $10d$–$15d$ from the jet exit. This region is generally considered as the axial location that signals the beginning of the far field. Although different values of the spreading rate were reported for the region after $10d$–$15d$, a common belief is that the spreading rate of a synthetic jet is significantly enhanced over a continuous jet in this region. This is attributed to an enhanced eddy viscosity resulting from the pulsed nature of a synthetic jet according to Krishnan and Mohseni [26]. However, their spreading rates were calculated based on velocity profiles that are less than $30d$ away from the jet exit. In the current study, we have extended the measurement of the flow field to $70d$–$100d$ from the orifice. Moreover, a curve fitting method described in Ref. [32] was adopted to enable accurate calculations of the jet half width and the centerline velocity from the measured velocity profile data. As a result, we observed notable variations of the spreading and decay rates in the axial direction.

The following part first presents the results for the spreading rate S_b, which is defined by $b_{1/2} = S_b(x - x_o)$. Here, $b_{1/2}$ is the jet half width, which is the radial distance between the jet centerline and the location where the axial velocity u is half of the centerline velocity u_c. Also, x denotes the axial location, and x_o is the location of the virtual origin (see Ref. [32] for details), which is an imaginary point on the x axis that the jet appears to linearly spread out. Now, the half-width data for six sample cases are plotted against the axial location in Fig. 1(a). We can observe that the slope of each fitted curve is the largest at the axial location around $20d$; however, the slope gradually decreases and

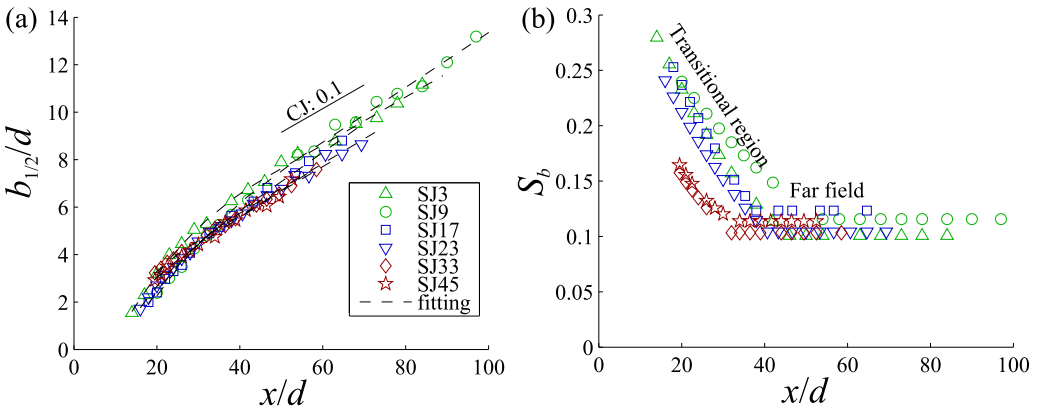

FIG. 1. (a) Axial variation of the jet half width $b_{1/2}$ for six different synthetic jets listed in Table I. The slope of a typical continuous jet (CJ) is also plotted for comparison. (b) Axial variation of the jet spreading rate S_b.

then saturates farther downstream (∼50d for SJ3 and SJ9, ∼40d for SJ17 and SJ23, and ∼30d for SJ33 and SJ45), where the fully developed far field begins. Since the slope of the curve physically indicates the spreading rate, the above observation can be quantitatively verified in Fig. 1(b), which shows the axial variations of the jet spreading rate for the same cases. Now, we can confirm the results from previous studies that the spreading rates of synthetic jets are indeed enhanced over that of conventional continuous jets (around 0.1 [34–37]) in the region after $x = 15d$. However, this enhancement does not persist throughout the downstream region, as the spreading rates reach asymptotic values that are comparable to continuous jets in the region after $x = 30d$–$50d$. Therefore, we propose that an extended transitional region should be identified for synthetic jets to account for the region that has a significantly enhanced and varying spreading rate. This enhanced spreading rate could be associated with the interaction of the pulsed vortical structures, as will be discussed later.

Another characteristic of synthetic jets is the decay of the centerline velocity, which is measured by the decay rate S_u, defined in $u_c = 1/[S_u(x - x_o)]$. Normally, the decay rate is a dimensional value so it is not readily comparable among different jets. In this study, a velocity scale U_K [32] is defined as $U_K = \sqrt{4K/(\pi d^2)}$, based on the constant far-field momentum flux K and the orifice diameter d for each individual jet. The axial variations of the scaled centerline velocity and the nondimensional decay rate are shown in Fig. 2. According to the decay behaviors, we can again confirm the existence

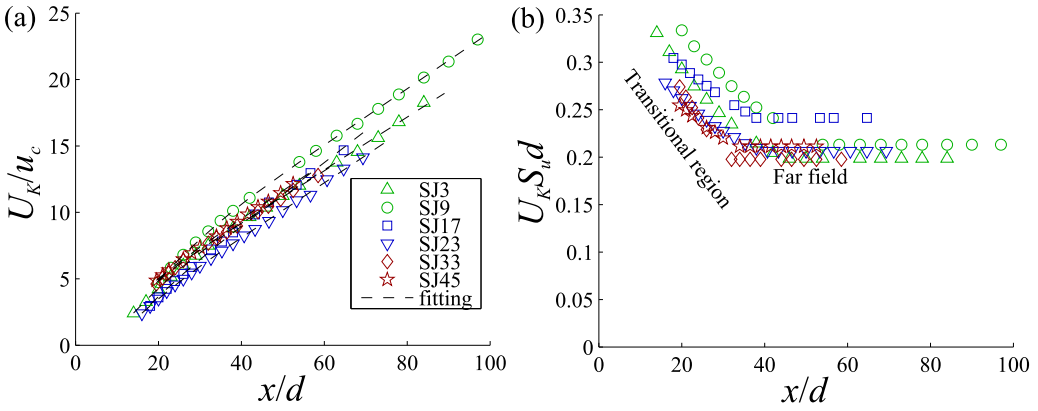

FIG. 2. (a) Axial variations of the inverted scaled centerline velocity for the same cases shown in Fig. 1. (b) Axial variations of the nondimensional decay rate.

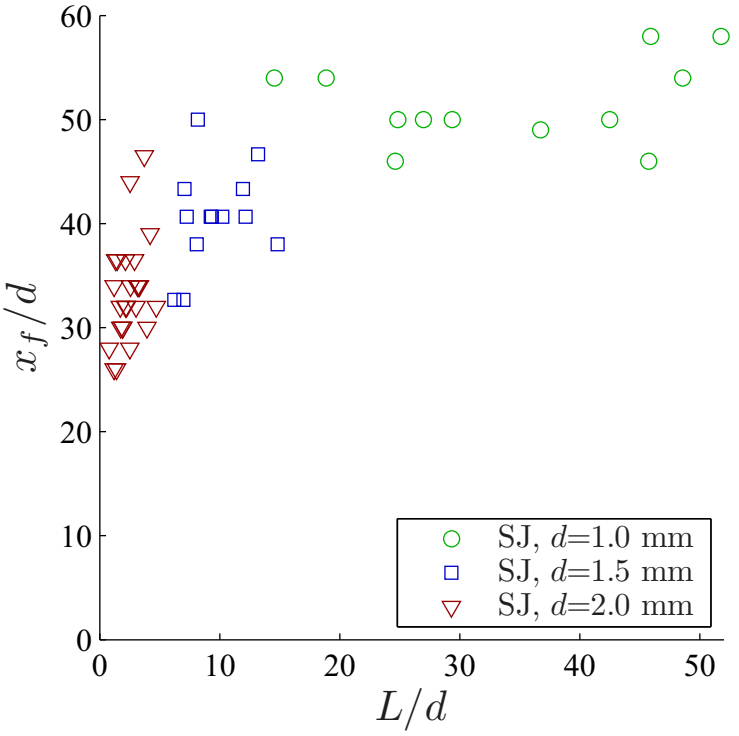

FIG. 3. The beginning of the far field x_f vs the stroke ratio L/d for 50 different synthetic jets reported in Ref. [32].

of a transitional region, which has a much enhanced decay rate over the far field. We also observe that the spreading and decay behaviors are qualitatively similar for all cases, by comparing Figs. 1 and 2. This observation clearly indicates that the spreading and decay behaviors of synthetic jets are coupled, which is consistent with the essence of the classical Schlitching jet [38] according to our recent study [31].

Based on Figs. 1 and 2, the beginning of the far field, denoted x_f, can be defined as the axial location where the spreading and decay rates saturate. Figure 3 plots x_f/d against the nondimensional stroke length L/d for the 50 different synthetic jets reported in Ref. [32]. The scattered data suggest that there might not be a sharp boundary between the transitional region and the far field in reality. Still, a general trend can be observed that x_f/d increases with L/d and tends to saturate around $50d$ as L/d increases. Specifically, for small L/d cases the axial dimension of the flow field has a positive correlation with the stroke length L, which is in reasonable agreement with the finding of Smith and Glezer [7] that the near-field flow of synthetic jets scales on L. For large L/d, it is likely that the far-field flow is less affected by varying stroke length because of the occurrence of vortex pinch-off [39], in which case the leading vortex ring stops growing and detaches from its feeding shear layer when L/d exceeds a threshold formation number. According to our previous study [32], the leading vortex ring is responsible for delivering the majority of the far-field momentum; thus, in the case L/d is larger than the formation number, the far-field flow becomes less sensitive to L/d because the leading vortex ring no longer grows with increasing L/d. Next, we shall focus on the fundamental mechanism governing the transitional region of a synthetic jet.

Physically, the enhanced spreading and decay behaviors in the transitional region of a synthetic jet are essentially caused by an enhanced pulsatile mixing within the jet, which can be modeled by an effective-eddy-viscosity concept [31]. To explain the source of the enhanced mixing for synthetic jets, we start with the case of a continuous turbulent jet, where turbulence is known as the primary

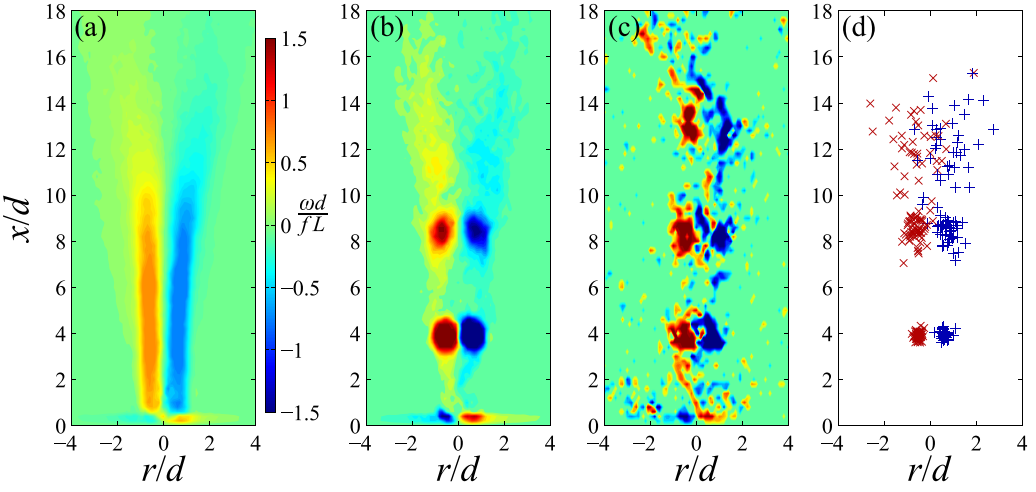

FIG. 4. (a) Mean vorticity contour for SJ33. ω is the vorticity, so $\omega d/fL$ is the nondimensional vorticity. (b) A sample phase-locked vorticity contour averaged over 50 different cycles of SJ33. (c) The instantaneous vorticity contour of a sample cycle corresponding to (b). (d) The locations of large vortices for the 50 different cycles of (b). The vortex locations are determined by the Q criterion [47].

mechanism that increases mixing beyond a laminar jet. Specifically, the mixing for a laminar jet is governed by the kinematic viscosity. However, as the jet evolves downstream, the laminar shear layer develops instabilities and grows to form large coherent vortical structures, which eventually break down into small eddies to form a turbulent flow [40–44]. Meanwhile, the kinematic viscosity of the mean flow escalates into the turbulent eddy viscosity as the nature of the flow grows from laminar to turbulent. This process suggests that the mixing intensity of the mean flow is related to the level of instability and disorder of the instantaneous flow [45].

Following the same idea, we present mean and phased-locked vorticity contours in Fig. 4 to demonstrate the unique mixing behaviors of a synthetic jet from an instability perspective. Figure 4(a) shows the mean vorticity contour of a synthetic jet and the near field ($x/d < 10$) can be identified by two strong shear layers. Figure 4(b) shows a sample phase-locked vorticity contour of the same synthetic jet averaged over different cycles. We can observe that the near field is characterized by coherent vortical structures that resemble the roll-up of shear layers between laminar and turbulent regions of a continuous jet. However, the difference is that the vortical structures of a synthetic jet are generated by external excitation (pulsation) as opposed to the natural instability of free shear layers. Therefore, the interaction, coalescence, and breakdown of the vortices of a synthetic jet should be dictated by the time and length scales related to the pulsation. As a result, an enhanced mode of instability is created in the transitional region ($x/d > 10$) of a synthetic jet, where large vortical structures still exist while their evolution becomes highly irregular and unpredictable. This is demonstrated in Figs. 4(c) and 4(d), which show the instantaneous vorticity field and the locations of coherent vortical structures obtained from the same phase of different cycles. Similar statistical observations for a two-dimensional synthetic jet were also reported by Béra *et al.* [46]. These results suggest that the instantaneous flow of the transitional region is vortical and fluctuating, while the mean flow is reduced to weak shear layers [see Fig. 4(a)] and displays near-turbulent jet features, e.g., the self-similarity. However, because the vortical structures in the transitional region are still large compared with the small eddies of an actual turbulent jet, the instability of those large vortices is likely to induce larger momentum transport than a turbulent flow. This explains why the mixing of the transitional region is enhanced over the far field, where the large vortical structures of a synthetic jet eventually break down into small eddies of an unforced turbulent flow.

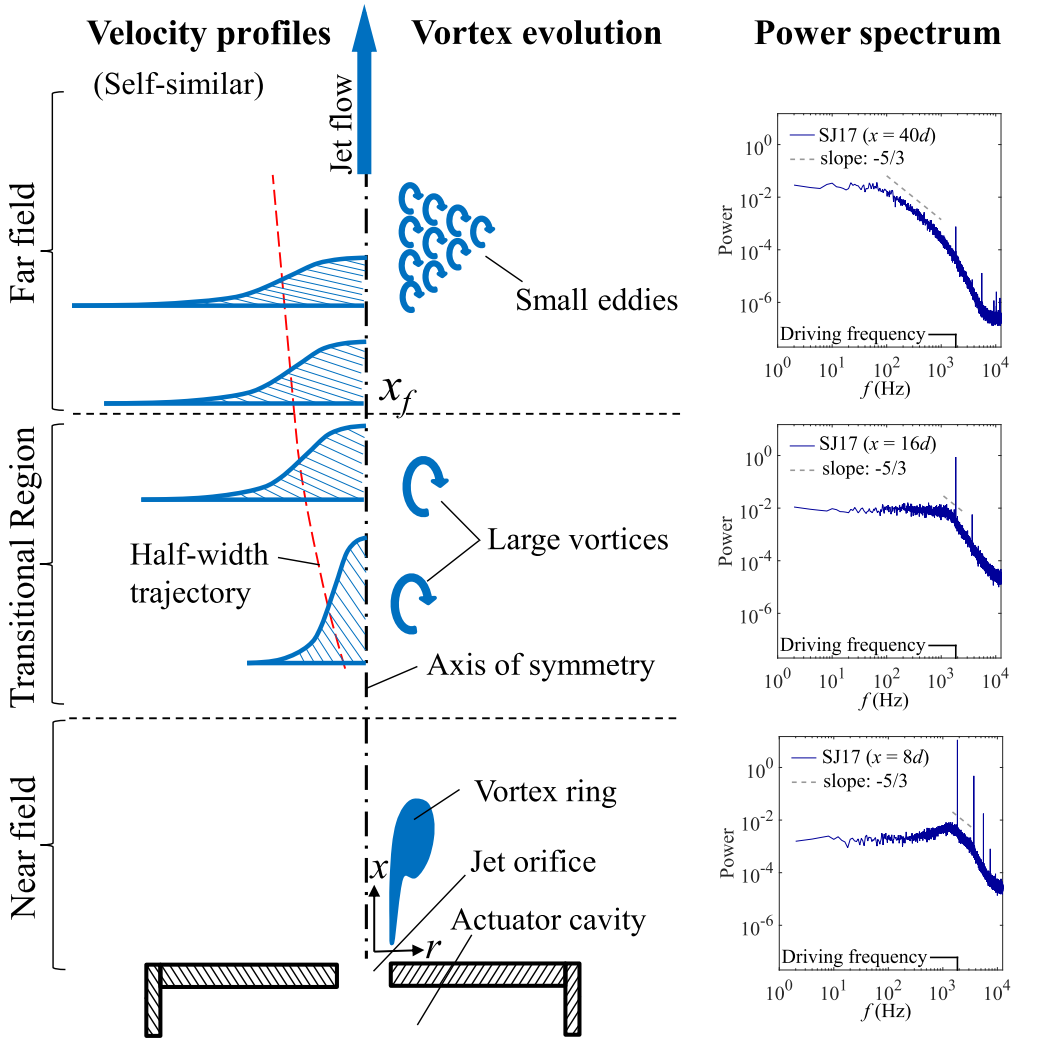

FIG. 5. The left schematic shows the mean velocity field and the corresponding vortical structures in different regions of a synthetic jet. The right figure presents the power spectrum results in different regions of a sample synthetic jet (SJ17).

To further substantiate the above understanding, Fig. 5 presents the power spectrum plots for the near field, transitional region, and far field of a sample synthetic jet (SJ17). In the near field, it is seen that the driving frequency coincides with the highest energy peak followed by its subharmonics. Since this is also the frequency at which the coherent vortex rings are generated, it justifies the dominance of the periodic flow induced by the main vortex rings. In the transitional region, the impact of the primary pulsation harmonic is gradually reduced while moving away from the orifice. Meanwhile, a Kolmogorov scaling of $-5/3$ emerges near the primary pulsation frequency, indicating the initiation of a turbulent flow regime dictated by the interaction of vortices at the corresponding length scale. This mechanism is similar to that of a continuous jet, except that the energy peaks for continuous jets correspond to the vortical structures that are formed due to natural instabilities. To this end, the special mixing mode of a synthetic jet is attributed to the special turbulent flow with "forced" instabilities. Moving further downstream into the far field shows the growth of the Kolmogorov

scaling region, while the effects of the pulsation harmonic and subharmonics diminish, marking the establishment of a fully developed turbulent flow.

To summarize, the current study focuses on the characteristics of the spreading and decay behaviors in the region beyond the near field of round synthetic jets. The results suggest the existence of an extended transitional region, as far as $30d$–$50d$ from the jet exit, where the spreading and decay rates are significantly enhanced over a continuous jet. This is attributed to an enhanced mixing of the transitional region caused by a forced instability of large vortical structures. However, as the large vortices break down into small eddies, the spreading and decay rates eventually decrease to asymptotic values comparable to a continuous jet in the far field. The information obtained from this work leads to an improved understanding and hypothesis of the flow regions of a round synthetic jet, as illustrated in Fig. 5. The near field is dominated by the periodic generation of coherent vortex rings. These vortex rings are relatively stable and their movements are predictable as they advect downstream under self-induced effect. In the transitional region, the main vortex rings become weaker and gradually decelerate so they begin to interact with each other. As a result, instability starts to kick in and the motions of the vortices become irregular. This is why the flow displays some turbulent features, i.e., the self-similar mean flow. However, the forced instability of these large vortical structures causes intense momentum transport and mixing, and consequently results in strong spreading and entrainment of the mean jet flow. As the vortical structures move further downstream and arrive at the fully developed far field, where the large vortices break down into smaller eddies, the transition into a full turbulent state is finally achieved and the appearance of the jet is not much different from the far field of a continuous jet.

This research was supported by the Air Force Office of Scientific Research. We would like to thank Dr. Adam DeVoria and Isaac J. Sledge for proofreading and providing helpful comments.

[1] A. Glezer and M. Amitay, Synthetic jets, Annu. Rev. Fluid Mech. **34**, 503 (2002).
[2] K. Mohseni and R. Mittal, *Synthetic Jets: Fundamentals and Applications* (CRC Press, Boca Raton, FL, 2014).
[3] H. Tang and S. Zhong, Simulation and modeling of synthetic jets, in *Vortex Rings and Jets*, edited by S. Yu (Springer, Berlin, 2016), pp. 93–144.
[4] M. Chiatto, F. Capuano, G. Coppola, and L. de Luca, LEM characterization of synthetic jet actuators driven by piezoelectric element: A review, Sensors **17**, 1216 (2016).
[5] J. E. Cater and J. Soria, The evolution of round zero-net-mass-flux jets, J. Fluid Mech. **472**, 167 (2002).
[6] J. P. Johnston and M. Nishi, Vortex generator jets—means for flow separation control, AIAA J. **28**, 989 (1990).
[7] B. L. Smith and A. Glezer, The formation and evolution of synthetic jets, Phys. Fluids **10**, 2281 (1998).
[8] R. Holman, Y. Utturkar, R. Mittal, B. L. Smith, and L. Cattafesta, Formation criterion for synthetic jets, AIAA J. **43**, 2110 (2005).
[9] J. Zhou, H. Tang, and S. Zhong, Vortex roll-up criterion for synthetic jets, AIAA J. **47**, 1252 (2009).
[10] T. Van Buren, E. Whalen, and M. Amitay, Vortex formation of a finite-span synthetic jet: High Reynolds numbers, Phys. Fluids **26**, 014101 (2014).
[11] B. L. Smith and G. W. Swift, Synthetic jets at larger Reynolds number and comparison to continuous jets, in *15th AIAA Computational Fluid Dynamics Conference*, AIAA paper 2001-3030 (AIAA, Reston, VA, 2001).
[12] B. L. Smith and G. W. Swift, A comparison between synthetic jets and continuous jets, Exp. Fluids **34**, 467 (2003).
[13] A. Seifert, S. Eliahu, and D. G. I. Wygnanski, Use of piezoelectric actuators for airfoil separation control, AIAA J. **36**, 1535 (1998).

[14] M. Amitay, D. R. Smith, V. Kibens, D. E. Parekh, and A. Glezer, Aerodynamic flow control over an unconventional airfoil using synthetic jet actuators, AIAA J. **39**, 361 (2001).
[15] T. Yehoshua and A. Seifert, Active boundary layer tripping using oscillatory vorticity generator, Aerosp. Sci. Technol. **10**, 175 (2006).
[16] R. Raju, R. Mittal, and L. Cattafesta, Dynamics of airfoil separation control using zero-net-mass-flux forcing, AIAA J. **46**, 3103 (2008).
[17] S. Zhang and S. Zhong, Experimental investigation of flow separation control using an array of synthetic jets, AIAA J. **48**, 611 (2010).
[18] L. N. Cattafesta and M. Sheplak, Actuators for active flow control, Annu. Rev. Fluid Mech. **43**, 247 (2011).
[19] J. Yen and N. A. Ahmed, Synthetic jets as a boundary vorticity flux control tool, AIAA J. **51**, 510 (2013).
[20] K. Mohseni, Pulsatile vortex generators for low-speed maneuvering of small underwater vehicles, Ocean Eng. **33**, 2209 (2006).
[21] M. Krieg and K. Mohseni, Thrust characterization of a bioinspired vortex ring thruster for locomotion of underwater robots, IEEE J. Oceanic Eng. **33**, 123 (2008).
[22] M. B. Gillespie, W. Z. Black, C. Rinehart, and A. Glezer, Local convective heat transfer from a constant heat flux flat plate cooled by synthetic air jets, J. Heat Transfer **128**, 990 (2006).
[23] A. Pavlolva and M. Amitay, Electronic cooling using synthetic jet impingement, J. Heat Transfer **128**, 897 (2006).
[24] X. M. Tan and J. Z. Zhang, Flow and heat transfer characteristics under synthetic jet impingement driven by piezoelectric actuator, Exp. Therm. Fluid Sci. **48**, 134 (2013).
[25] X. He, J. A. Lustbader, M. Arik, and R. Sharma, Heat transfer characteristics of impinging steady and synthetic jets over vertical flat surface, Int. J. Heat Mass Transfer **80**, 825 (2015).
[26] G. Krishnan and K. Mohseni, Axisymmetric synthetic jets: An experimental and theoretical examination, AIAA J. **47**, 2273 (2009).
[27] R. Rathnasingham and K. Breuer, Coupled fluid-structural characteristics of actuators for flow control, AIAA J. **35**, 832 (1997).
[28] S. G. Mallinson, G. Hong, and J. A. Reizes, Some characteristics of synthetic jets, in *30th Fluid Dynamics Conference*, AIAA paper 99-3651 (AIAA, Reston, VA, 1999).
[29] J. M. Shuster and D. R. Smith, Experimental study of the formation and scaling of a round synthetic jet, Phys. Fluids **19**, 045109 (2007).
[30] X. Xia and K. Mohseni, An experimental and modeling investigation of synthetic jets in a coflow wake, Int. J. Flow Control **3**, 19 (2011).
[31] X. Xia and K. Mohseni, Parameter governing the far-field features of round jets, Phys. Rev. Fluids **1**, 062401 (2016).
[32] X. Xia and K. Mohseni, Far-field momentum flux of high-frequency axisymmetric synthetic jets, Phys. Fluids **27**, 115101 (2015).
[33] X. Xia and K. Mohseni, Flow characterization and modeling of strong round synthetic jets in crossflow, AIAA J. **55**, 389 (2017).
[34] S. P. Capp, Experimental investigation of the turbulent axisymmetric jet, Ph.D. thesis, University at Buffalo, SUNY, Buffalo, NY, 1983.
[35] D. Peng, Hot wire measurements in a momentum conserving axisymmetric jet, Master's thesis, University at Buffalo, SUNY, Buffalo, NY, 1985.
[36] N. R. Panchapakesan and J. L. Lumley, Turbulence measurements in axisymmetric jets of air and helium. Part 1. Air jet, J. Fluid Mech. **246**, 197 (1993).
[37] H. J. Hussein, S. P. Capp, and W. K. George, Velocity measurements in a high Reynolds number, momentum conserving, axisymmetric, turbulent jet, J. Fluid Mech. **258**, 31 (1994).
[38] H. Schlichting, *Boundary Layer Theory*, 2nd ed. (McGraw-Hill, New York, 1955).
[39] M. Gharib, E. Rambod, and K. Shariff, A universal time scale for vortex ring formation, J. Fluid Mech. **360**, 121 (1998).
[40] S. C. Crow and P. H. Champagne, Orderly structure in jet turbulence, J. Fluid Mech. **48**, 547 (1971).
[41] G. Brown and A. Roshko, On density effects and large structure in turbulent mixing layers, J. Fluid Mech. **64**, 775 (1974).

[42] A. J. Yule, Large-scale structure in the mixing layer of a round jet, J. Fluid Mech. **89**, 413 (1978).
[43] J. Cohen and I. Wygnanski, The evolution of instabilities in the axisymmetric jet. Part 1. The linear growth of disturbances near the nozzle, J. Fluid Mech. **176**, 191 (1987).
[44] T. H. Weisgraber and D. Liepmann, Turbulent structure during transition to self-similar in a round jet, Exp. Fluids **24**, 210 (1998).
[45] C. M. Ho and P. Huerre, Perturbed free shear layers, Annu. Rev. Fluid Mech. **16**, 365 (1984).
[46] J. C. Béra, M. Michard, N. Grosjean, and G. Comte-Bellot, Flow analysis of two-dimensional pulsed jets by particle image velocimetry, Exp. Fluids **31**, 519 (2001).
[47] P. Chakraborty, S. Balachandar, and R. J. Adrian, On the relationships between local vortex identification schemes, J. Fluid Mech. **535**, 189 (2005).